Tasman Sea biological response to dust storm events during the austral spring of 2009.

A.J.Gabric[1], R.Cropp[1], G.McTainsh[1], H.Butler[2], B.Johnston[3], T.O'Loingsigh[1] and Dien Van Tran[1]

[1]School of Environment, Griffith University, Nathan, Qld, 4111.

[2] School of Agricultural, Computational & Environmental Sciences, University of Southern Queensland, Toowoomba, Qld, 4350

[3] School of Natural Science, Griffith University, Nathan, Qld, 4111.

Abstract

During the austral spring of 2009 several significant dust storms occurred in SE Australia including the so-called 'Red Dawn' event in late September. Estimates of 2.5 Mt total suspended particulate sediment lost off the Australian coast in the 3000 km long dust plume, make it the largest off-continent loss of soil ever reported. Much of this material was transported over the coastline of New South Wales and into the adjacent Tasman Sea. Long term model simulations of dust deposition over the southwest Tasman Sea suggest the amount deposited during the spring of 2009 was about three-times the long term monthly average. Previous satellite-based analyses of the biological response of Tasman Sea waters to dust-derived nutrients are equivocal or have observed no response. Satellite-derived surface chlorophyll concentrations in the southern Tasman during the spring of 2009 are well above the climatological mean, with positive anomalies as high as 0.5 mg m^{-3}. Dust transport simulations indicate strong deposition to the ocean surface, which during both the 'Red Dawn' event and mid-October 2009 dust storm events was enhanced by heavy precipitation. Cloud processing of the dust aerosol may have enhanced iron bioavailability for phytoplankton uptake.

Keywords : phytoplankton, dust storms, Tasman Sea, Australia

Introduction

Aeolian deposition of nutrient-rich dust has been shown to stimulate phytoplankton growth in various oligotrophic oceanic regions of the Northern Hemisphere (Bishop *et al.* 2002; Harrison *et al.* 1999; Lenes *et al.* 2001). Although the evidence is limited, event-based analyses in waters proximal to the Australian continent have shown similar phytoplankton responses to dust deposition in the Southern Ocean south of Australia (Gabric *et al.* 2010), and in subtropical waters off southern Queensland (Shaw *et al.* 2008). However, other event-based studies have found little or no phytoplankton response to even major dust storm events in Australian waters (Mackie *et al.* 2008). Taking a climatological approach, Cropp *et al*. (2013) analysed a 20-year record of air parcel trajectories from the Lake Eyre Basin (LEB) in central Australia, and argued that marine biological receptivity to dust-derived nutrients is seasonally variable, and often not in synchrony with the timing of dust deposition. Cropp *et al.* (2013) suggest this may explain why some large dust storm events have not always produced a clear phytoplankton response in ocean waters adjacent to the continent.

Dust storm frequency in Australia is strongly seasonal and related to wind conditions, rainfall, and vegetation patterns, with peak dust storm activity in northern Australia occurring during spring and early summer, and activity in southern Australia reaching a maximum during summer (McTainsh and Leys 1993). Dust from Australian continental sources such as the LEB is entrained by warm pre-frontal northerly winds, frontal westerlies and post-frontal southerlies (Strong *et al.* 2010) and transported either to the north-west over the Indian Ocean, south over the Southern Ocean, or southeast over the Tasman Sea in association with the west-to-east passage of cold fronts (McTainsh 1998). During the austral spring and summer, the northerly migration of the band of cold fronts contributes to increased dust storm activity over south-eastern Australia (McTainsh, 1998) and increases the likelihood of dust deposition over the adjacent oceans. Dust deposition events in the Subantarctic Southern Ocean have resulted in strong phytoplankton growth (Gabric *et al.* 2010), however, analyses of dust deposition over the Tasman Sea have not revealed a similar phytoplankton response (Mackie *et al.* 2008).

An anomalously intense dust storm event on 22 and 23 September 2009, called "Red Dawn" by the media, most likely originated in the southern LEB, the Strzelecki sub-basin and western and central New South Wales (NSW) and was the largest to pass over Sydney, Australia (as measured by its effect on visibility) since records began in 1940. Estimates of 2.54 Mt total suspended particulate sediment lost off the Australian coast in the 3000 km long dust plume, make it the largest off-continent loss of soil ever reported (Leys *et al.* 2011). The vertical distribution of dust from lidar

satellite data and analysis of model results also indicate that significant amounts of dust aerosols were transported over the Tasman Sea toward New Zealand (Choobari *et al.* 2012). Mineralogical analyses of the Red Dawn event showed the dust's elemental composition included high amounts of Si (24%) and Fe (6%), with 50% of the particles in the <10 μm particle size range, indicating long-range transport from source (Aryal *et al.* 2012).

Presented here is a detailed analysis of the marine biological response in the Tasman Sea from 25-40°S during September–October, 2009. The impact of dust deposition to the ocean surface is evaluated using satellite-derived estimates of phytoplankton biomass, as indicated by surface chlorophyll (CHL), and atmospheric aerosol burden, indicated by aerosol optical depth (AOD). To examine the impact on the Tasman Sea, we have simulated contemporaneous atmospheric dust load and deposition over the Tasman using a regional dust transport model that provides daily data for the study period.

Materials and Methods

Study Region Characteristics

Lying between the Coral Sea and the Southern Ocean, the Tasman Sea (Fig. 1) spans the latitudes 30–50°S, extending over 2800 km north–south, and includes sub-tropical to Subantarctic water masses (Anon. 1953). The main geostrophic feature along the eastern continental shelf is the East Australian Current (EAC), which flows southward until near 32°S where it detaches from the coast (Godfrey *et al.* 1980; Ridgway and Dunn 2003). The EAC then veers east between 32°S and 34°S to form the Tasman Front, where it flows across the Tasman Sea (Suthers *et al.* 2011). The hydrodynamic situation south of the Tasman Front is complex with a large number of mesoscale eddies, some semi-permanent features, originating within the EAC, and termed the 'Eddy Avenue' (Everett *et al.* 2012), that can significantly affect the local phytoplankton biomass (Everett *et al.* 2012; Suthers *et al.* 2011). Cyclonic (upwelling) eddies within this eddy field have almost double the CHL (0.35 mg m^{-3}) of anticyclonic eddies (0.18 mg m^{-3}) (Everett *et al.* 2012). Observations from a long-term ocean station off eastern Tasmania show that the southward penetration of the EAC has increased over the past 60 years (Ridgway 2007).

Spanning such a large meridional area, the Tasman Sea is characterised by high spatial heterogeneity in biological activity. Macro-nutrients are low in the northern sub-tropical region (Ellwood *et al.* 2013), but high in the southern Tasman (Bowie *et al.* 2011). Longhurst (2007) states that the

southern Tasman (east of Tasmania) exhibits a typical spring bloom with CHL maximal in late September or early October. However, interannual variability in CHL is high with the bloom onset varying by as much as four months at a fixed location. Satellite-derived climatologies of CHL in the northern Tasman Sea show a peak in winter (May–October), decreasing to low levels from November to April. In March, high CHL is concentrated in the Subtropical Convergence zone near 40^{o}S (Hayes *et al.* 2005).

Silicate concentrations along the east coast of the Australian continent are low (typically < 2μM) and have declined in recent decades (Condie and Dunn 2006; Thompson *et al.* 2009), possibly due to a change in the long-term supply from southward-flowing EAC water (Ridgway 2007). The role of Fe in mediating macro-nutrient uptake in phytoplankton is well documented with growth rates low in Fe-depleted regions (de Baar *et al.* 1999; Timmermans *et al.* 2004). Given the significant decline in surface silicate over the period 1947–2004, both Fe and silicate co-limitation may affect phytoplankton growth in the Tasman Sea, and the occasional deposition of Fe and silicate-rich dust may promote diatoms blooms. In a meridional transect from 33–43^{o}S during summer, Hassler et al. (2014) note that cyanobacteria dominate in subtropical waters of the northern Tasman Sea, with non-diazotroph phytoplankton nitrogen limited. This contrasted with the subantarctic water mass in the southern Tasman Sea, where the phytoplankton community was dominated by a bloom of haptophytes. The low productivity in the subantarctic zone was explained by light limitation, but nitrogen, silicic acid, as well as Fe, were all depleted to the extent that they could become co-limiting. We note that *Trichodesmium spp.*, dinitrogen-fixing cyanobacteria, often form extensive blooms in subtropical ocean waters off north-eastern Australia (Carpenter *et al.* 1992). However, of relevance here, is that *Trichodesmium*, unlike other phytoplankton, are able to mediate dust dissolution, most likely via reduction(Rubin *et al.* 2011). Several field studies document the ability of *Trichodesmium* to utilize Fe by accelerating the rate of Fe dissolution from oxides and dust, through as yet unspecified cell-surface processes (Rubin *et al.* 2011; Shaked and Lis 2012).

Analysis of ocean colour data reveals that the Tasman Sea contains the largest non-coastal surface CHL concentrations within the South Pacific Ocean, with the variability in phytoplankton concentrations linked to mesoscale eddies (Tilburg *et al.* 2002). Upwelling and downwelling associated with these eddies can increase vertical mixing and nutrient concentrations in the upper ocean. Generally, high-phytoplankton concentrations are confined either to cold-core cyclonic eddies or along the coast, where upwelling can transport nutrients into the euphotic zone and stimulate phytoplankton growth (Suthers *et al.* 2011). High resolution eddy-resolving modelling suggests enhanced eddy activity with climate change may increase the nutrient supply to the upper

ocean and cause an increase in the phytoplankton concentrations and primary productivity by 10% in the western Tasman Sea (Matear *et al.* 2013).

Long-term measurements at an inshore location, Port Hacking (similar to 34^{o}S), show a phytoplankton community that is dominated by diatoms during spring and with maximal CHL between August–October (Thompson et al. 2009). SeaWiFS CHL anomalies show substantial (~+100% of monthly mean) episodic blooms occur at Port Hacking, with notable events in August 1998, October 2002 and January 2007. Although these are not convincingly explained, there is some evidence that dust-derived nutrients are a causative factor in the increased frequency of coastal phytoplankton blooms in NSW (Ajani *et al.* 2011).

Based on analysis of dust storm seasonality and aeolian transport from the continent, the likelihood of dust deposition over the Tasman Sea is relatively low from January through August, moderate during early spring, September–October, and low from November–December (Cropp et al. 2013). However, Cropp et al. (2013) found that ocean biological receptivity (as measured by mixed layer CHL and irradiance) to an injection of atmospheric nutrients is low during spring, so that a bloom is unlikely to develop at this time. This is consistent with analysis of a dust storm that passed over the southern Tasman during October 2003 and that produced no discernible phytoplankton response 7 to 30 days after the dust storm (Boyd et al. 2004; Mackie et al. 2008).

A dust storm during early February 2005 coincided with sampling in the northern Tasman (in the vicinity of the Tasman Front) and although there was an increase in mixed layer (ML) iron (Fe) concentrations, no increase in primary production post-dust deposition was observed (Ellwood *et al.* 2013). Field data collected in the north-eastern Tasman (~29°S, 170°E) in March–April, 2006 during and after a cyclone, showed elevated surface ocean inventories of Fe, suggestive of a dust source, which was probably enhanced by anomalously high wet deposition (Law *et al.* 2011). Shipboard dust-addition experiments showed that diazatrophic nitrogen fixation increased by an order of magnitude (Law *et al.* 2011). The observed ten-fold increase in nitrogen fixation in situ exceeded that reported in other nutrient perturbation experiments despite comparatively low concentrations of in situ dissolved Fe, indicating that Fe bioavailability may be a critical factor in determining the phytoplankton response to dust-derived nutrients in the Tasman Sea.

The bioavailability of Fe in the ocean requires it to be in a soluble form as one precondition, and Fe in mineral dust is typically insoluble (Mackie *et al.* 2008). However, the factors affecting Fe dissolution are multiple and complex, and include its different possible phases (particulate, colloidal, soluble), and the presence of Fe-binding ligands, which may lead to a redefinition of the term

157 'dissolved iron' (Breitbarth *et al.* 2010). Jickells and Spokes (2001) report that overall solubility of
158 aerosol Fe at seawater pH is 0.8–2.1% of the total Fe deposited, however, wet-deposited mineral
159 aerosols had a much higher soluble Fe (14%) than dry deposited. The influence of aerosol cloud
160 processing on enhancing Fe solubility has been noted in several studies (Shi *et al.* 2009; Shi *et al.*
161 2012; Zhang *et al.* 2013).

162 ### *Dust event observations*

163 The reduction in atmospheric visibility during a dust storm, or other dust entrainment event, is
164 referred to as dust visibility reduction (DVR), and this can be used as a quantitative measure of the
165 intensity of an event (Gabric *et al.* 2010). DVR is computed as follows:

166 $DVR = V_{max} - V_{rec}$,

167 where, V_{max} is the upper limit of measured visibility (50 km) as used by Australian Bureau of
168 Meteorology (ABM) observers, and V_{rec} is the recorded visibility associated with the dust event. DVR
169 provides a numerical value for dust entrainment event intensity (from 0 to 50km) without the need
170 to classify events into different types. The DVR data is presented as a cumulative total of those
171 observer stations recording an event (rather than an average across stations) because, in our opinion
172 this is a better way of illustrating the combined effects of the frequency and intensity of dust
173 entrainment events. High cumulative DVR values, therefore, indicate that many ABM stations were
174 recording dust and that most of these stations recorded severe dust conditions. DVR data was
175 gathered from a total of 138 observing stations which included those in Queensland south of
176 latitude 23.3 degrees (Rockhampton), and all stations in NSW.

177 ### *Dust transport and deposition model*

178 The connection between individual dust storm events in southern Australia and resultant deposition
179 over the adjacent ocean was investigated using the integrated wind erosion and dust transport
180 model (CEMSYS) to simulate the daily deposition during Sept–Dec 2009. The CEMSYS model has
181 been used for modelling several dust storms in Australia (Lu and Shao 2001; Shao and Leslie 1997)
182 and was successfully validated using concurrent dust concentration data for a major dust storm
183 event that moved north-east over the continent during October 2002 (McTainsh *et al.* 2005; Shao *et*
184 *al.* 2007). CEMSYS is a process-based model which couples an atmospheric sub-model, a wind
185 erosion sub-model, and a dust transport and deposition sub-model. These sub-models are supported
186 by a GIS database. The structure and details of the various sub-models is outlined in Shao and Leslie

(1997) and Lu and Shao (2001). CEMSYS takes into account the atmospheric conditions (wind speed, rainfall and temperature), soil conditions (soil texture and soil water) and surface vegetation.

For this study, CEMSYS was run at 0.45° x 0.45° resolution over the domain 108°E–168.75°E, 8.1°S–57.6°S, which covers the Australian continent, Southern Ocean and Tasman Sea for the simulation period. Atmospheric conditions used in the CEMSYS simulations for each day in the simulation period were obtained from HIRES, a High Resolution limited area atmospheric prediction model developed by Leslie (1998). Land surface information required for the CEMSYS simulations is summarised in Table 1. It was assumed that vegetation cover was slowly varying and therefore constant for each month in the simulation. Vegetation cover for each month was estimated based on each month's Leaf Area Index (LAI) calculated from MODIS NDVI data using the empirical relationships developed by McVicar et al. (1996b). Soil texture across the continent was divided up into USDA soil texture classes. Each soil class was characterised by a particle-size density function. The particle-size distributions of each soil class were considered to be unchanged during wind erosion events. Soil moisture varied considerably during the simulation period and was modelled accordingly within CEMSYS (Shao *et al.* 2007).

Satellite Data

The Tasman Sea sub-region selected for the satellite data analysis covers 25–40°S and 150–170°E and includes the area under the path of the Red Dawn dust plume. Strictly, the northern extent of our study region extends into the Coral Sea as the Tasman's northern boundary is defined as 30°S (Anon. 1953). Daily and 8-day MODIS (Aqua) binned CHL and AOD data at 550-nm and 4-km resolution are retrieved for the period September–December 2009. The study region is divided into five-degree latitude bands for statistical analysis. Climatological mean CHL is derived from the available MODIS 8-day archive (2002–2013) and anomalies are computed from this mean. Rainfall rate data at a resolution of 0.25° latitude-longitude are obtained from the Special Sensor Microwave/Imager (SSM/I) archive maintained by Remote Sensing Systems and sponsored by the NASA Earth Science MEaSUREs Program (www.remss.com).

Results and Discussion

Synoptic Meteorology and Dust Deposition

Fig. 2a shows the synoptic mean sea level barometric pressure charts just before and during the 'Red Dawn' dust storm event from 22–25 September 2009 (days of the year 265–268). On 22 and 23

September 2009, a broad area of low pressure dominated south-eastern Australia, while a cold front stretched from 28–37°S and a large low pressure trough stretched from 12– 35°S. With the passage of the trough and the cold front from west to east, wind direction over the LEB and western NSW changed from north or north-westerly to south-west and westerly (Leys *et al.* 2011). During and prior to the 'Red Dawn' event, winds recorded in the western part of NSW were between 80 and 100 km/h and elevated dust was recorded at numerous Dustwatch stations across NSW on 22 and 23 September (http://www.environment.nsw.gov.au/resources/dustwatch/DWNL090928.pdf).

MODIS Terra pseudo-true colour imagery captured for September 22–23 (Fig. 3a) show the passage and extent of the dust plume as it crosses the coast and moves north-east over the Tasman Sea. The dust is clearly entrained in north-westerly winds associated with a cyclonic system to the south (Fig. 3b). On 25 September a subsequent cold front passed over the same region. Of relevance to the subsequent pattern of dust deposition over the Tasman Sea, is the intense cyclonic system centred at approximately at 40°S, 165°E on 23 and 24 of September (Fig. 2).

The sum of the DVR values during September–October 2009 from all observing stations which recorded a dust event (including multiple daily DVR records when they occurred) is shown in Fig. 4a. Of the 61 days in September and October 2009, 40 days (or 65.5%) were dusty somewhere in the defined monitoring region. The most active day was September 23 when 107 (or 77.5%) of 138 stations recorded dust. The 'Red Dawn' event was followed by two smaller events in late September/early October, plus another dust storm (61 stations involved) in mid-October as shown in the DVR time series for the September–October period (Fig. 4a).

The Hovmoller plot of the CEMSYS simulated dust deposition (Fig. 5b-c) shows strong deposition between 25–35°S (Fig. 5b-d) on day 266 (Sept 23), following the 'Red Dawn' dust storm on day 265, and also further south (30–40°S) on day 268 (Sept 25). This confirms that the dust plume transport was driven by the cyclonic low pressure system which was centred on the Tasman Sea between 35-40°S on the 23 September (Fig. 2), transported north to south and then likely rained out. Another strong dust deposition event is simulated on days 286–287 (October 13–14) with dust again deposited over a large latitude band, especially east of 155°E (Fig. 5b-d).

Fig. 6a-b show the 3-day average rainfall rate for 22–24 Sept and 13–15 October from the SSM/I sensor, and confirms widespread precipitation over the Tasman Sea on both occasions. Fig. 6c-d show the CEMSYS simulated proportion of wet deposition for these two periods, confirming that extensive wet deposition occurred over the southern Tasman, particularly during the September event. As noted above, cloud processing of the dust aerosol followed by wet deposition likely

enhanced the deposition rates and the solubility of dust-derived Fe deposited to the ocean during these events.

Satellite AOD and CHL

The MODIS AOD daily time series (Fig. 4b) shows a strong spike from 22–24 September, which is remarkable as the AOD values were averaged over the entire Tasman study region. The MODIS 3-day average AOD (Fig. 4c) confirms the extensive impact of the dust plume on AOD and atmospheric aerosol burden.

To illustrate the meridional change in bloom phenology in the Tasman, the climatological mean monthly CHL derived from the MODIS archive is presented in five-degree latitude bands in Fig. 7. The CHL peak occurs later in the year with increasing latitude; the timing of peak CHL ranging from August in subtropical waters to December, south of 40^{o}S. The magnitude of the seasonal CHL peak also increases markedly with latitude, from 0.23 mg m^{-3} in subtropical waters to 0.47 mg m^{-3} in the subantarctic zone.

Hovmoller latitude-time plots of MODIS 8-day CHL concentrations and climatology (Fig. 8a-b) show that the phytoplankton response seems to be largely confined to the south of the Tasman Front, at approximately 32^{o}S (Fig. 8c, 9c), with the greatest positive anomalies (>0.6 mg m^{-3}) occurring south of 35^{o}S between days 270-280, even though deposition was simulated further north (Fig. 5). Assuming that dust-derived Fe stimulated the phytoplankton response, this is consistent with the observations of Ellwood et al. (2013) who suggested that Fe was unlikely to limit primary production north of the Tasman Front. Alternatively, it may also suggest that the dust-derived Fe deposited in the northern Tasman was less soluble and therefore less available for phytoplankton.

Baseline Dust Inputs to the Tasman Sea

Fig. 10 shows the annual dust deposition (g m^{-2}yr^{-1}) from a previous CEMSYS model simulation for the period 2001–2011 in the region 30-45^{o}S, 145-154^{o}E (shown as shaded in the map insert), which includes the southwest Tasman Sea and subantarctic waters to the south. Although this area excludes the northern and eastern Tasman, which were affected by dust from the Red Dawn event, the seasonality and episodic nature of dust storm events is clear, with 2009 the fourth highest annual deposition in the time series. The mean dust deposited over the southwest Tasman during the spring of 2009 was 0.17 Mt per month, which is almost three times the long-term average monthly dust deposition of 0.063 ± 0.10 Mt and underscores the intensity of the 2009 dust storm season.

It is interesting to estimate the amount of dust-derived Fe that was delivered to the Tasman surface waters during the Red Dawn event. Table 2 gives the CEMSYS modelled dust deposition for 22-25 September 2009, in ten 3°x3° cells that cover most of the Tasman Sea. There are clear spatial gradients in deposition with higher values near the Australian coast, and in the northern Tasman. The east-west spatial gradient in modelled deposition is broadly consistent with the satellite data on AOD given in Figure 4c, bearing in mind that the relationship between dust loading, satellite AOD and dust deposition is complex. Assuming a mean depositional flux of $1x10^{-8}$ g $m^{-2}s^{-1}$ and an Fe content of 3.5% for Australian dust (Mackie *et al.* 2005), this equates to a flux of $3.5x10^{-10}$ g $m^{-2}s^{-1}$ of particulate Fe, corresponding to a delivery of 0.12 mg Fe m^{-2} over the four-day Red Dawn period. By way of comparison, Jickells *et al.* (2005) use the results from three modelling studies to derive a composite estimate of annual dust deposition over the Tasman Sea in range 0.2–1 g m^{-2} yr^{-1} (≅ 0.6 – 3 x 10^{-8} g m^{-2} s^{-1}). It is also interesting to note that the deposition flux over the Tasman during the Red Dawn event was a factor of five higher than that modelled over the Subantarctic Southern Ocean during the very active 2002 dust storm season (Gabric *et al.* 2010).

The September-November period coincides with rapid shoaling of the ML in the Tasman, from 160m to 40m (Tilburg *et al.* 2002). Assuming an ocean ML depth of 100m during late September, the ML particulate Fe concentration would be 0.0012 mg m^{-3}. However, given a typical oceanic vertical mixing coefficient of 10^{-4} $m^{-2}s^{-1}$ it would take approximately 12 days for a conservative tracer to be mixed uniformly over a 100m ML, which is unlikely for particulate Fe, given dissolution and rapid uptake by phytoplankton (Bowie *et al.* 2009). A more reasonable estimate of the particulate Fe concentration in the upper 10m of the water column is 0.012 mg m^{-3} or 0.21 nmole L^{-1}. This compares with observed surface values of particulate Fe of about 0.05—0.2 nmole L^{-1} in the subantarctic zone, measured at Station P3 (46°S, 153°E) during January–February 2007 (Bowie *et al.* 2009). Interestingly, there was quite low dust storm deposition over the SW Tasman Sea during 2007 (see Fig. 10).

Perhaps the largest uncertainty in such estimates is the solubility and bioavailability of this particulate Fe. A broad range of physical, chemical and biological factors can affect dust-derived Fe solubility in both the marine atmosphere and upper ocean (Baker and Croot 2008). Jickells and Spokes (2001) report that overall solubility of aerosol Fe at seawater pH for wet deposited mineral aerosols is a much higher than for dry deposited (14% compared with about 1%), which was indeed the situation in the southern Tasman during the Red Dawn event (see Fig 6). A physical control on aerosol Fe solubility has been suggested by Baker and Jickells (2006), namely the preferential removal of larger particles during long-range transport leading to reduced modal size of the dust

population. Such smaller dust particles have a correspondingly larger surface area to volume ratio, and hence a greater proportion of their Fe content close enough to the particle surface to dissolve. Given the source area for the dust likely being the LEB (over 1000km west of Sydney), the approximate distance travelled by the dust plume to the northern Tasman was well over 2000km, and almost 3000km for those dust particles transported first northeast across the coast, and then from north to the south by the cyclonic system centred at between 35–40^{o}S. The theory proposed by Baker and Jickells (2006) suggests that dust-derived Fe transported the longer distance to the southern Tasman will be more soluble and hence elicit a greater phytoplankton response. Both mechanisms affect the solubility of particulate Fe and could help explain the contrasting phytoplankton responses observed between the northern and southern Tasman Sea (Figs 8 and 9).

Chlorophyll Anomalies

The mid-October deposition event simulated around day 286 seems to promote a widespread, CHL response between days 290–295, which is again confined to the south of 32^{o}S. CHL concentrations achieved during these events are well above the climatological mean values for spring, with positive anomalies as high as 0.5 mg m^{-3}. As noted above, the ocean ML depth decreases rapidly through October, so that light would be less important in limiting of phytoplankton growth at this time.

The CHL anomaly Hovmoller plot by longitude shows high inshore anomalies occur throughout the spring season north of 35^{o}S (Fig. 9a–b), which are likely due to eddy pumping or coastal upwelling. Figure 11 shows sea-level height anomalies (left-panel) and SST (right panel) for September 24. The penetration of warm EAC waters well south of the Tasman Front with entrainment of warm waters in an inshore eddy at 36^{o}S is notable. The SST data clearly show both warm core (36^{o}S, 153^{o}E) and cold core (33^{o}S, 156^{o}E) eddies, which persisted for several days in the satellite record (IMOS 2009). However, the large offshore extent of positive CHL anomalies south of 35^{o}S (Fig. 9c), strongly suggest the CHL increase post the Red Dawn event was due to the deposition of dust.

Fig. 12a–b show the spatial distribution of CHL anomalies (mg m^{-3}) in the octad periods following the 'Red Dawn' and mid-October dust storm events. The basin-wide extent of these plumes of elevated CHL suggests that phytoplankton biomass increased over a large part of the Tasman Sea, that could not be caused by localized enhanced nutrient supply from coastal upwelling or cyclonic eddy pumping, since both processes are confined to waters in the western Tasman and closer to the NSW coast (Fig. 11). Taken together with the timing of simulated dust deposition this points to dust-derived nutrients as the most likely cause.

Conclusions

We have presented various data on ocean surface CHL, atmospheric aerosol loading (from AOD) and atmospheric dust deposition (modelled) over the Tasman Sea to explore the connection between the austral spring dust storm season of 2009, and the biogeochemical response of the adjacent ocean. Continental observations of DVR and dust transport model simulations suggest the deposition of dust to the Tasman Sea was significant, albeit episodic, and enhanced by widespread precipitation, during the late September and mid-October events.

The two dust storms that traversed the south-east coast of Australia during late September and mid-October 2009 appear to have caused a widespread spike in phytoplankton biomass in the Tasman Sea, especially south of the Tasman Front. Although the 'Red Dawn' event of late September was one of the largest in the record in terms of total soil loss, the biological response was almost as strong following the less intense mid-October event, suggesting the timing and mode of delivery of dust-derived nutrients and ocean state are all critical factors. Both events were accompanied by widespread precipitation over the Tasman Sea which is thought to enhance the solubility of dust associated Fe. A previous 20-year climatological analysis of dust storm trajectories suggested that an asynchrony between deposition and ocean receptivity in the Tasman Sea would make such events rare (Cropp *et al.* 2013), which underscores the unusual nature of the 2009 dust storm season.

Surface CHL concentrations observed during the study period are well above the climatological mean for this time of the year, with positive anomalies as high as 0.5 mg m^{-3}. Although we do not have observations of in situ Fe concentration during spring 2009, results from other studies suggest that Fe can limit phytoplankton growth south of the Tasman Front, which is where the greatest phytoplankton response was seen. It is also clear that multiple factors, such as the mode of deposition (wet versus dry), dust solubility, and scavenging of released Fe all interact to set the seawater concentration of bioavailable Fe (Boyd and Ellwood 2010).

It is anticipated that as a result of global warming droughts will become more frequent and the number of severe dust storms in Australia may as a consequence increase (Bhattachan and D'Odorico 2014). There is some evidence that the mean aerosol loading over the continent is already changing due to enhanced dust storm activity (Mitchell *et al.* 2010). Although our data describe a very active dust storm season, they raise the possibility that future enhanced delivery of Australian dust to the Tasman Sea under warming may have significant impacts on regional phytoplankton dynamics and the carbon sink of these waters.

Acknowledgements:

The data presented in Figs 4 b and 4c in this paper were produced with the Giovanni online data system, developed and maintained by the NASA GES DISC. The SSM/I data shown in Fig. 6 were produced by Remote Sensing Systems (www.remss.com) and sponsored by the NASA Earth Science MEaSUREs DISCOVER Project. Data was sourced from the Integrated Marine Observing System (IMOS) - IMOS is supported by the Australian Government through the National Collaborative Research Infrastructure Strategy and the Super Science Initiative.

References

Ajani, P., Ingleton, T., Pritchard, T., and Armand, L. (2011) Microalgal Blooms in the Coastal Waters of New South Wales, Australia. *Proceedings of the Linnean Society of New South Wales* **133**, 15-31.

Anon. (1953) Limits of Oceans and Seas. Monaco.

Aryal, R., Kandel, D., Acharya, D., Chong, M.N., and Beecham, S. (2012) Unusual Sydney dust storm and its mineralogical and organic characteristics. *Environmental Chemistry* **9**(6), 537-546.

Baker, A.R., and Croot, P.L. (2008) Atmospheric and marine controls on aerosol iron solubility in seawater. *Marine Chemistry* **doi:10.1016/j.marchem.2008.09.003**.

Baker, A.R., and Jickells, T.D. (2006) Mineral particle size as a control on aerosol iron solubility. *Geophysical Research Letters* **33**(17), L17608.

Bhattachan, A., and D'Odorico, P. (2014) Can land use intensification in the Mallee, Australia increase the supply of soluble iron to the Southern Ocean? *Scientific Reports* **4**.

Bishop, J.K.B., Davis, R.E., and Sherman, J.T. (2002) Robotic observations of dust storm enhancement of carbon biomass in the North Pacific. *Science* **298**(5594), 817-821.

Bowie, A.R., Griffiths, F.B., Dehairs, F., and Trull, T.W. (2011) Oceanography of the subantarctic and Polar Frontal Zones south of Australia during summer: Setting for the SAZ-Sense study. *Deep-Sea Research Part Ii-Topical Studies in Oceanography* **58**(21-22), 2059-2070.

Bowie, A.R., Lannuzel, D., Remenyi, T.A., Wagener, T., Lam, P.J., Boyd, P.W., Guieu, C., Townsend, A.T., and Trull, T.W. (2009) Biogeochemical iron budgets of the Southern Ocean south of Australia: Decoupling of iron and nutrient cycles in the subantarctic zone by the summertime supply. *Global Biogeochemical Cycles* **23**.

Boyd, P.W., and Ellwood, M.J. (2010) The biogeochemical cycle of iron in the ocean. *Nature Geoscience* **3**(10), 675-682.

Breitbarth, E., Achterberg, E.P., Ardelan, M.V., Baker, A.R., Bucciarelli, E., Chever, F., Croot, P.L., Duggen, S., Gledhill, M., Hassellov, M., Hassler, C., Hoffmann, L.J., Hunter, K.A., Hutchins, D.A., Ingri, J., Jickells, T., Lohan, M.C., Nielsdottir, M.C., Sarthou, G., Schoemann, V., Trapp, J.M., Turner, D.R., and Ye, Y. (2010) Iron biogeochemistry across marine systems - progress from the past decade. *Biogeosciences* **7**(3), 1075-1097.

Carpenter, E.J., Capone, D.G., and Rueter, J.G. (Eds) (1992) 'Marine Pelagic Cyanobacteria: Trichodesmium and other Diazotrophs.' (Springer Science and Business Media)

Choobari, O.A., Zawar-Reza, P., and Sturman, A. (2012) Atmospheric forcing of the three-dimensional distribution of dust particles over Australia: A case study. *Journal of Geophysical Research-Atmospheres* **117**.

Condie, S.A., and Dunn, J.R. (2006) Seasonal characteristics of the surface mixed layer in the Australasian region: implications for primary production regimes and biogeography. *Marine and Freshwater Research* **57**(6), 569-590.

Cropp, R.A., Gabric, A.J., Levasseur, M., McTainsh, G.H., Bowie, A., Hassler, C., Law, C., McGowan, H., Tindale, N., and Viscarra Rossel, R. (2013) The likelihood of observing dust-stimulated phytoplankton growth in waters proximal to the Australian continent. *Journal of Marine Systems* **117**, 43-52.

de Baar, H.J.W., de Jong, J.T.M., Nolting, R.F., Timmermans, K.R., van Leeuwe, M.A., Bathmann, U., van der Loeff, M.R., and Sildam, J. (1999) Low dissolved Fe and the absence of diatom blooms in remote Pacific waters of the Southern Ocean. *Marine Chemistry* **66**(1-2), 1-34.

Ellwood, M.J., Law, C.S., Hall, J., Woodward, E.M.S., Strzepek, R., Kuparinen, J., Thompson, K., Pickmere, S., Sutton, P., and Boyd, P.W. (2013) Relationships between nutrient stocks and inventories and phytoplankton physiological status along an oligotrophic meridional transect in the Tasman Sea. *Deep-Sea Research Part I-Oceanographic Research Papers* **72**, 102-120.

Everett, J.D., Baird, M.E., Oke, P.R., and Suthers, I.M. (2012) An avenue of eddies: Quantifying the biophysical properties of mesoscale eddies in the Tasman Sea. *Geophysical Research Letters* **39**.

Gabric, A.J., Cropp, R.A., McTainsh, G.H., Johnston, B.M., Butler, H., Tilbrook, B., and Keywood, M. (2010) Australian dust storms in 2002-2003 and their impact on Southern Ocean biogeochemistry. *Global Biogeochemical Cycles* **24**.

Godfrey, J.S., Cresswell, G.R., Golding, T.J., and Pearce, A.F. (1980) The separation of the East Australian Current. *Journal of Physical Oceanography* **10**(3), 430-440.

Harrison, P.J., Boyd, P.W., Varela, D.E., and Takeda, S. (1999) Comparison of factors controlling phytoplankton productivity in the NE and NW subarctic Pacific gyres. *Progress in Oceanography* **43**(2-4), 205-234.

Hassler, C.S., Ridgway, K.R., Bowie, A.R., Butler, E.C.V., Clementson, L.A., Doblin, M.A., Davies, D.M., Law, C., Ralph, P.J., van der Merwe, P., Watson, R., and Ellwood, M.J. (2014) Primary productivity induced by iron and nitrogen in the Tasman Sea: an overview of the PINTS expedition. *Marine and Freshwater Research* **65**(6), 517-537.

Hayes, D., Lyne, V., Condie, S., Griffiths, B., Pigot, S., and Hallegraeff, G. (2005) Collation and Analysis of Oceanographic Datasets for National Marine Bioregionalisation. A report to the Australian Government, National Oceans Office. (CSIRO Marine Research)

IMOS (2009) Integrated Marine Observing System. http://oceancurrent.imos.org.au/. Accessed 8 February 2015

Jickells, T.D., An, Z.S., Andersen, K.K., Baker, A.R., Bergametti, G., Brooks, N., Cao, J.J., Boyd, P.W., Duce, R.A., Hunter, K.A., Kawahata, H., Kubilay, N., laRoche, J., Liss, P.S., Mahowald, N., Prospero, J.M., Ridgwell, A.J., Tegen, I., and Torres, R. (2005) Global iron connections between desert dust, ocean biogeochemistry, and climate. *Science* **308**(5718), 67-71.

Jickells, T.D., and Spokes, L. (2001) Atmospheric iron inputs to the oceans. In The biogeochemistry of iron in seawater. (Eds. DR Turner and K Hunter) pp. 85-122. (John Wiley and Sons: New York Chichester)

Law, C.S., Woodward, E.M.S., Ellwood, M.J., Marriner, A., Bury, S.J., and Safi, K.A. (2011) Response of surface nutrient inventories and nitrogen fixation to a tropical cyclone in the southwest Pacific. *Limnology and Oceanography* **56**(4), 1372-1385.

Lenes, J.M., Darrow, B.P., Cattrall, C., Heil, C.A., Callahan, M., Vargo, G.A., Byrne, R.H., Prospero, J.M., Bates, D.E., Fanning, K.A., and Walsh, J.J. (2001) Iron fertilization and the Trichodesmium response on the West Florida shelf. *Limnology and Oceanography* **46**(6), 1261-1277.

Leslie, L. (1998) Weather forecasting models. In Climate Prediction for Agricultural and Resource Management,. (Eds. R Munro and L Leslie) pp. 103-116. (Bureau of Resource Sciences: Canberra.)

Leys, J.F., Heidenreich, S.K., Strong, C.L., McTainsh, G.H., and Quigley, S. (2011) PM10 concentrations and mass transport during "Red Dawn" - Sydney 23 September 2009. *AEOLIAN RESEARCH* **3**(3), 327-342.

Longhurst, A.R. (2007) 'Ecological Geography of the Sea.' 2nd edn. (Academic Press: San Diego)

Lu, H., and Shao, Y.P. (2001) Toward quantitative prediction of dust storms: an integrated wind erosion modelling system and its applications. *Environmental Modelling & Software* **16**(3), 233-249.

Mackie, D.S., Boyd, P.W., Hunter, K.A., and McTainsh, G.H. (2005) Simulating the cloud processing of iron in Australian dust: pH and dust concentration. *Geophysical Research Letters* **32**(6).

Mackie, D.S., Boyd, P.W., McTainsh, G.H., Tindale, N.W., Westberry, T.K., and Hunter, K.A. (2008) Biogeochemistry of iron in Australian dust: From eolian uplift to marine uptake. *Geochemistry Geophysics Geosystems* **9**.

510 Matear, R.J., Chamberlain, M.A., Sun, C., and Feng, M. (2013) Climate change projection of the
511 Tasman Sea from an Eddy-resolving Ocean Model. *Journal of Geophysical Research-Oceans* **118**(6),
512 2961-2976.

513
514 McTainsh, G., Chan, Y.C., McGowan, H., Leys, J., and Tews, K. (2005) The 23rd October 2002 dust
515 storm in eastern Australia: characteristics and meteorological conditions. *Atmospheric Environment*
516 **39**(7), 1227-1236.

517
518 McTainsh, G.H., A.W. Lynch, E.K. Tews (1998) Climatic controls upon dust storm occurrence in
519 eastern Australia. *J. Arid Environment* **39**, 457-466.

520
521 McTainsh, G.H., and Leys, J.F. (1993) Wind erosion. In Land Degradation Processes in Australia. (Eds.
522 GH McTainsh and WC Boughton). (Longman Chesire, Melbourne)

523
524 McVicar, T., Walker, J., Jupp, D., Pierce, L., Byrne, G., and Dallwitz, R. (1996a) Relating AVHRR
525 vegetation indices to in situ measurements of leaf area index. CSIRO Division of Water Resources,
526 Canberra.

527
528 McVicar, T.R., Walker, J., Jupp, D., Pierce, L., Byrne, G.T., and Dallwitz, R. (1996b) 'Relating AVHRR
529 vegetation indices to in situ measurements of leaf area index.' (CSIRO Division of Water Resources)

530
531 Mitchell, R.M., Campbell, S.K., and Qin, Y. (2010) Recent increase in aerosol loading over the
532 Australian arid zone. *Atmospheric Chemistry and Physics* **10**(4), 1689-1699.

533
534 Raupach, M.R. (1994) Simplified Expressions for Vegetation Roughness Length and Zero-Plane
535 Displacement as Functions of Canopy Height and Area Index. *Boundary-Layer Meteorology* **71**(1-2),
536 211-216.

537
538 Ridgway, K.R. (2007) Long-term trend and decadal variability of the southward penetration of the
539 East Australian Current. *Geophysical Research Letters* **34**(13).

540
541 Ridgway, K.R., and Dunn, J.R. (2003) Mesoscale structure of the mean East Australian Current System
542 and its relationship with topography. *Progress in Oceanography* **56**(2), 189-222.

543
544 Rubin, M., Berman-Frank, I., and Shaked, Y. (2011) Dust- and mineral-iron utilization by the marine
545 dinitrogen-fixer Trichodesmium. *Nature Geoscience* **4**(8), 529-534.

546
547 Shaked, Y., and Lis, H. (2012) Disassembling iron availability to phytoplankton. *Frontiers in*
548 *Microbiology* **3**.

549
550 Shao, Y.P., and Leslie, L.M. (1997) Wind erosion prediction over the Australian continent. *Journal of*
551 *Geophysical Research-Atmospheres* **102**(D25), 30091-30105.

Shao, Y.P., Leys, J.F., McTainsh, G.H., and Tews, K. (2007) Numerical simulation of the October 2002 dust event in Australia. *Journal of Geophysical Research-Atmospheres* **112**(D8).

Shaw, E.C., Gabric, A.J., and McTainsh, G.H. (2008) Impacts of aeolian dust deposition on phytoplankton dynamics in Queensland coastal waters. *Marine and Freshwater Research* **59**(11), 951-962.

Shi, Z.B., Krom, M.D., Bonneville, S., Baker, A.R., Jickells, T.D., and Benning, L.G. (2009) Formation of Iron Nanoparticles and Increase in Iron Reactivity in Mineral Dust during Simulated Cloud Processing. *Environmental science & technology* **43**(17), 6592-6596.

Shi, Z.B., Krom, M.D., Jickells, T.D., Bonneville, S., Carslaw, K.S., Mihalopoulos, N., Baker, A.R., and Benning, L.G. (2012) Impacts on iron solubility in the mineral dust by processes in the source region and the atmosphere: A review. *Aeolian Research* **5**, 21-42.

Strong, C.L., Parsons, K., McTainsh, G.H., and Sheehan, A. (2010) Dust transporting wind systems in the lower Lake Eyre Basin, Australia *AEOLIAN RESEARCH* **doi:10.1016/j.aeolia.2010.11.001**.

Suthers, I.M., Everett, J.D., Roughan, M., Young, J.W., Oke, P.R., Condie, S.A., Hartog, J.R., Hobday, A.J., Thompson, P.A., Ridgway, K., Baird, M.E., Hassler, C.S., Brassington, G.B., Byrne, M., Holbrook, N.J., and Malcolm, H.A. (2011) The strengthening East Australian Current, its eddies and biological effects - an introduction and overview. *Deep-Sea Research Part Ii-Topical Studies in Oceanography* **58**(5), 538-546.

Thompson, P.A., Baird, M.E., Ingleton, T., and Doblin, M.A. (2009) Long-term changes in temperate Australian coastal waters: implications for phytoplankton. *Marine Ecology Progress Series* **394**, 1-19.

Tilburg, C.E., Subrahmanyam, B., and O'Brien, J.J. (2002) Ocean color variability in the Tasman Sea. *Geophysical Research Letters* **29**(10).

Timmermans, K.R., van der Wagt, B., and de Baar, H.J.W. (2004) Growth rates, half-saturation constants, and silicate, nitrate, and phosphate depletion in relation to iron availability of four large, open-ocean diatoms from the Southern Ocean. *Limnology and Oceanography* **49**(6), 2141-2151.

Zhang, T.R., Shi, J.H., Gao, H.W., Zhang, J., and Yao, X.H. (2013) Impact of source and atmospheric processing on Fe solubility in aerosols over the Yellow Sea, China. *Atmospheric Environment* **75**, 249-256.

593 Table 1: Summary of land surface information used in the CEMSYS simulations.

Parameter	**Data Source**
Aerodynamic Roughness	Constant for bare soil Derived from vegetation height and LAI for vegetated surfaces (Raupach 1994)
Zero-displacement height	Zero for bare soil Derived from vegetation height and LAI for vegetated surfaces (McVicar *et al.* 1996a)
Leaf Area Index (LAI)	Derived from SeaWiFS NDVI data
Vegetation Height	Adapted from the Atlas of Australia Resources
Soil particle-size distribution	Particle-size analysis of selected soil samples
Soil moisture	Soil moisture model integrated into CEMSYS.

594

595

596 Table 2: CEMSYS simulated mean dust depositional flux (g $m^{-2}s^{-1}$) during Red Dawn event

Longitude / Latitude	150-153ºE	153-156ºE	156-159ºE	159-162ºE	162-165ºE
31-34ºSº	4.7 $x10^{-8}$	3.2 $x10^{-8}$	1.8 $x10^{-8}$	1.0 $x10^{-8}$	1.0 $x10^{-8}$
34-37ºS	0.96 $x10^{-8}$	0.61 $x10^{-8}$	0.55 $x10^{-8}$	0.48 $x10^{-8}$	0.48 $x10^{-8}$

597

598

FIGURE CAPTIONS

Figure 1 Tasman Sea study region (EAC: East Australian Current; STF: subtropical front)

Figure 2 Synoptic pressure charts for Sept 22–25, 2009 (www.bom.gov.au)

Figure 3 True colour image of 'Red Dawn' dust plume from MODIS Terra overpass on 23 Sept 2009 at (a) 00:05 UTC and, (b) 23:10 UTC on the 23 September 2009

Figure 4 (a) Total DVR from ABM stations in Eastern Australia during September and October 2009, (b) Time series of daily areal average aerosol optical depth from MODIS (at 550nm), and (c) AOD over the Tasman Sea during 'Red Dawn' event

Figure 5 Hovmoller plot of CEMSYS simulated deposition (μg m^2s^{-1}) by longitude bands

Figure 6 SSM/I F17 three-day mean rainfall rate (mm hr^{-1}) for (a) September 23–25, 2009 and (b) October 13–15, 2009 (source: www.remss.com), and CEMSYS simulated proportion of wet deposition for (c) September 23–25, 2009 and (d) October 13–15, 2009

Figure 7 MODIS-derived chlorophyll climatology (2002–13) for the Tasman Sea by latitude band, averaged over 150–170°E.

Figure 8 Hovmoller plot of MODIS 8-day mean CHL data and 10-year climatology, by latitude averaged over 150–170°E.

Figure 9 Hovmoller plot of MODIS 8-day mean CHL anomalies, by longitude (150–170°E) averaged over the given latitude bands.

Figure 10 CEMSYS modelled long-term dust deposition time series for the southwest Tasman Sea as shown in the map insert.

Figure 11 Satellite sea level anomalies (left panel) and 3-day SST composite (right panel) for September 24, 2009 (from the IMOS, 2009 archive).

Figure 12 MODIS 8-day CHL anomalies (mg m^{-3}) for (a) 30 Sep –7 Oct, 2009, and (b) 16–23 Oct, 2009.

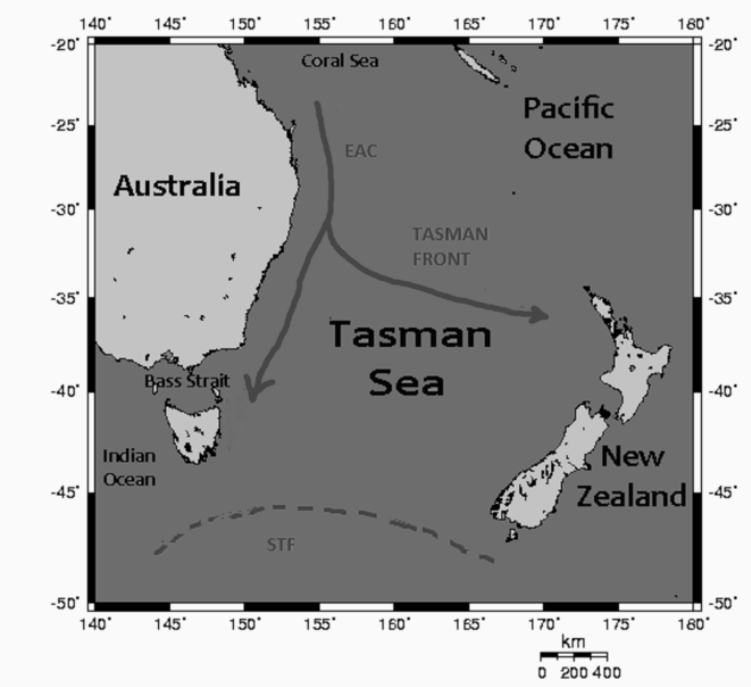

626

627 Fig. 1

628

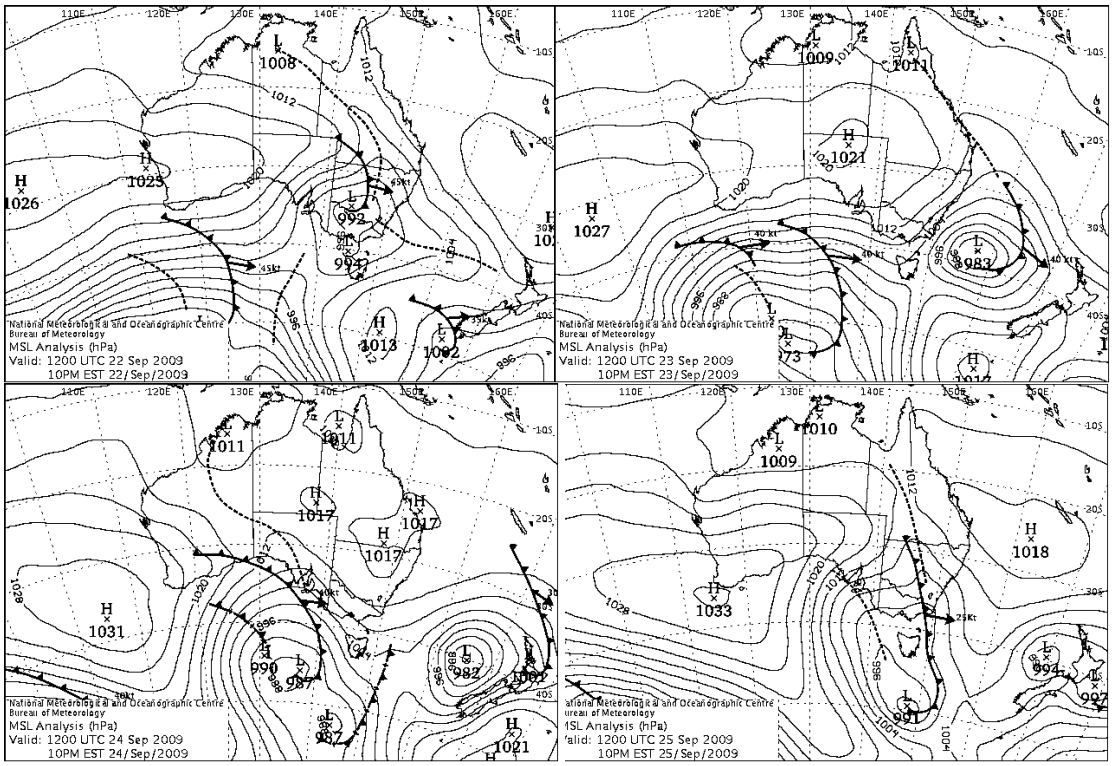
National Meteorological and Oceanographic Centre
Bureau of Meteorology
MSL Analysis (hPa)
Valid: 1200 UTC 22 Sep 2009
10PM EST 22/Sep/2009
National Meteorological and Oceanographic Centre
Bureau of Meteorology
MSL Analysis (hPa)
Valid: 1200 UTC 23 Sep 2009
10PM EST 23/Sep/2009
National Meteorological and Oceanographic Centre
Bureau of Meteorology
MSL Analysis (hPa)
Valid: 1200 UTC 24 Sep 2009
10PM EST 24/Sep/2009
National Meteorological and Oceanographic Centre
Bureau of Meteorology
MSL Analysis (hPa)
Valid: 1200 UTC 25 Sep 2009
10PM EST 25/Sep/2009

Fig. 2

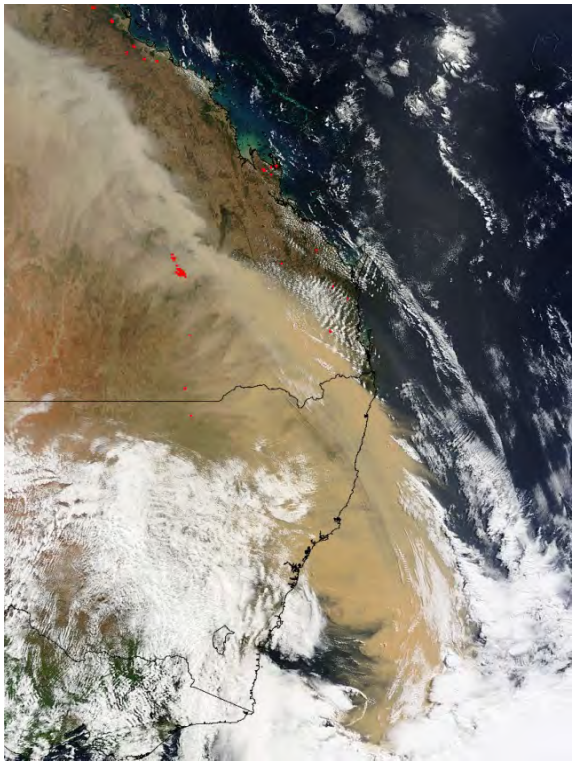

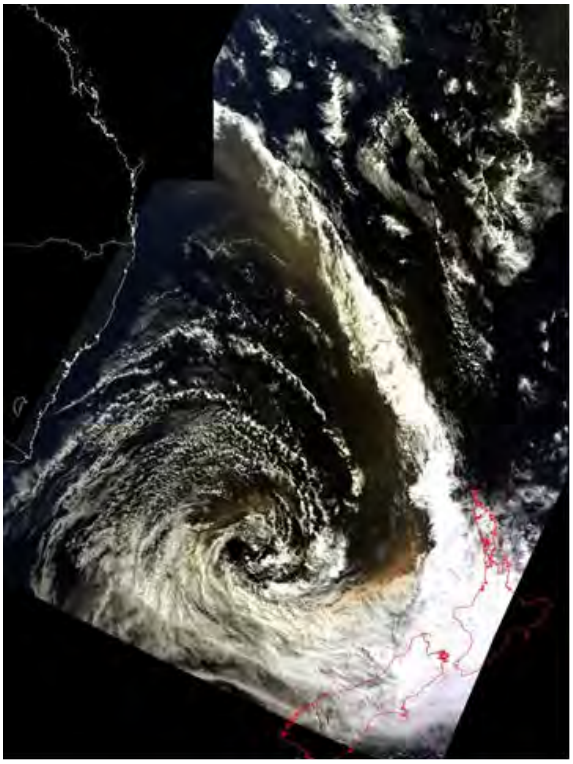

(a)

Fig. 3

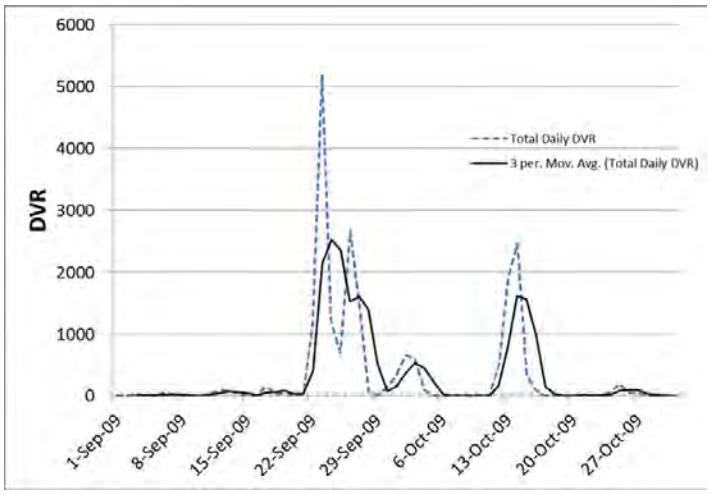
6000
5000
4000
3000
2000
1000
0
DVR
Total Daily DVR
3 per. Mov. Avg. (Total Daily DVR)
1-Sep-09
8-Sep-09
15-Sep-09
22-Sep-09
29-Sep-09
6-Oct-09
13-Oct-09
20-Oct-09
27-Oct-09

(a)

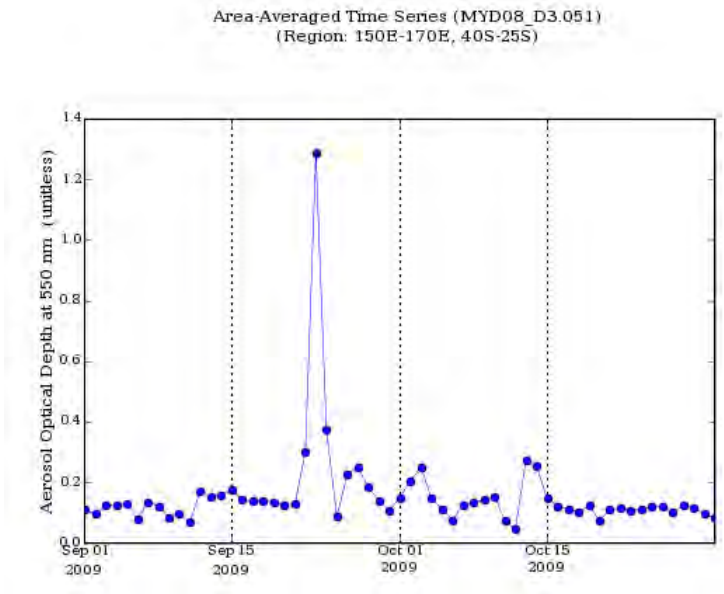
Area-Averaged Time Series (MYD08_D3.051)
(Region: 150E-170E, 40S-25S)
Aerosol Optical Depth at 550 nm (unitless)
1.4
1.2
1.0
0.8
0.6
0.4
0.2
0.0
Sep 01
2009
Sep 15
2009
Oct 01
2009
Oct 15
2009

(b)

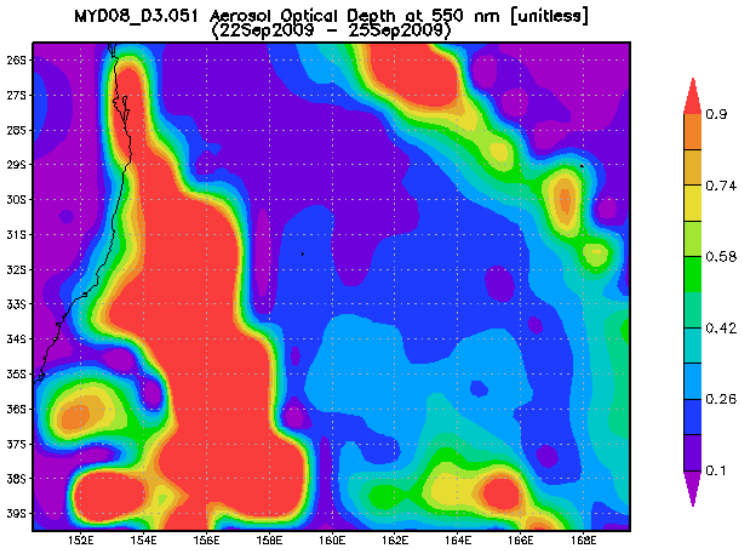
MYD08_D3.051 Aerosol Optical Depth at 550 nm [unitless]
(22Sep2009 - 25Sep2009)
26S
27S
28S
29S
30S
31S
32S
33S
34S
35S
36S
37S
38S
39S
152E
154E
156E
158E
160E
162E
164E
166E
168E
0.9
0.74
0.58
0.42
0.26
0.1

(c)

Fig. 4

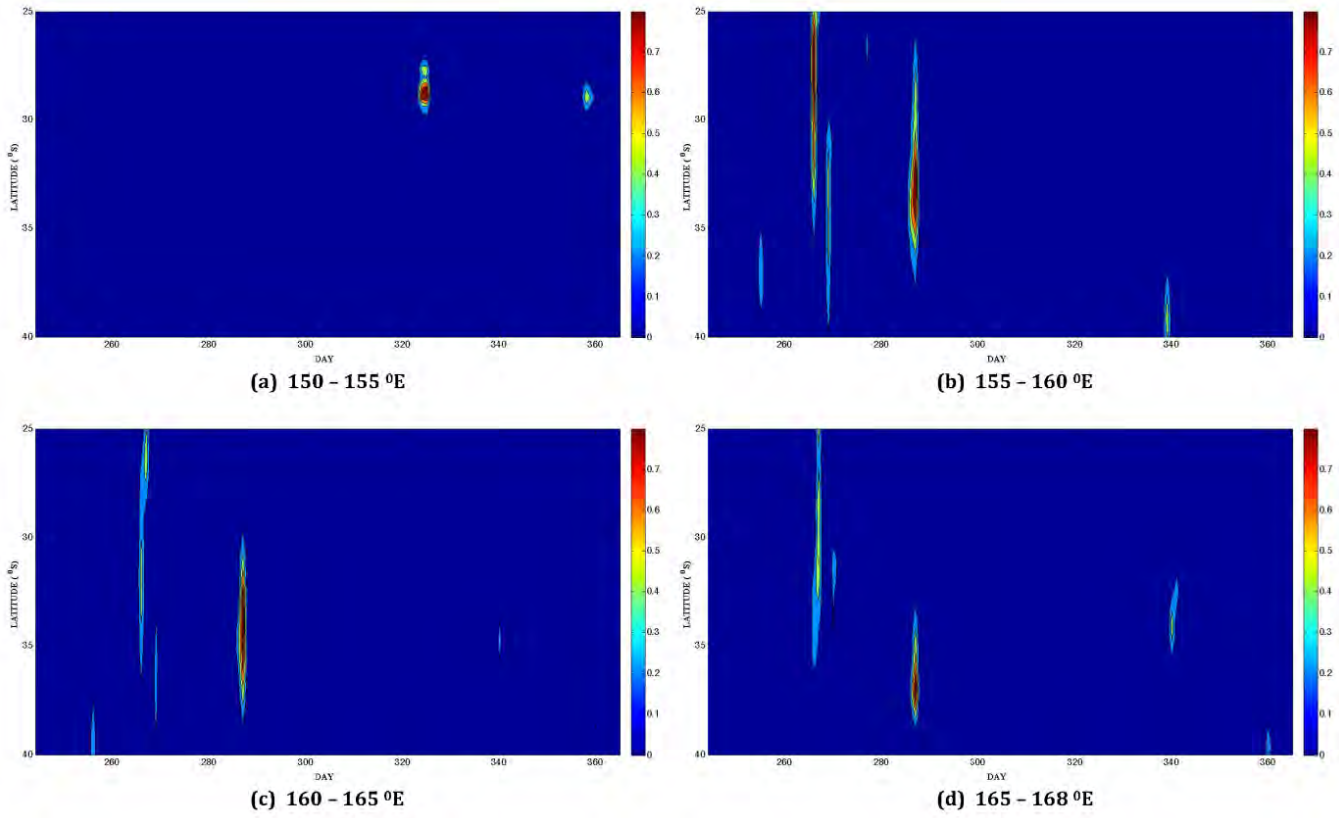

Fig. 5

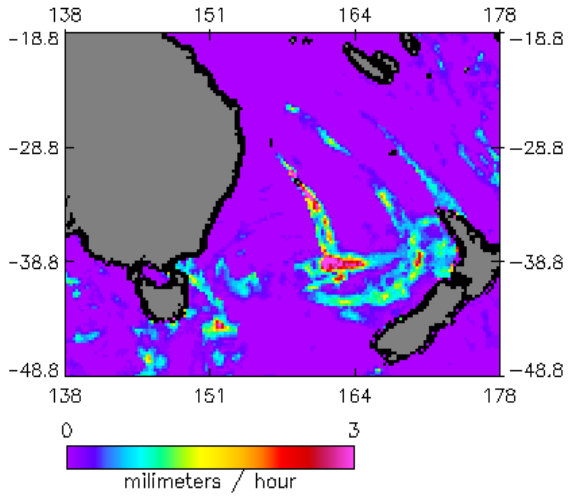
138
151
164
178
-18.8
-28.8
-38.8
-48.8
0
3
milimeters / hour

(a)

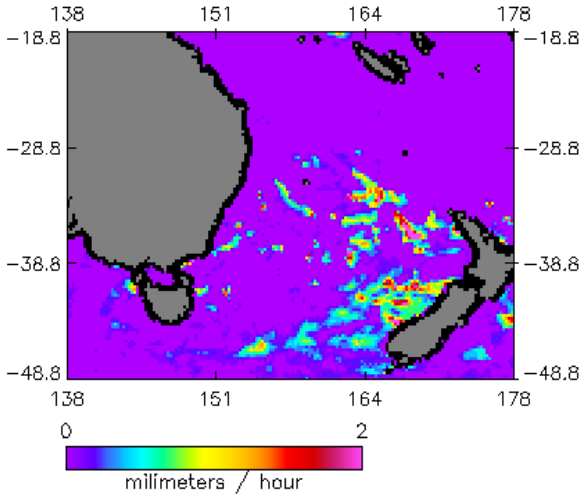
138
151
164
178
-18.8
-28.8
-38.8
-48.8
0
2
milimeters / hour

(b)

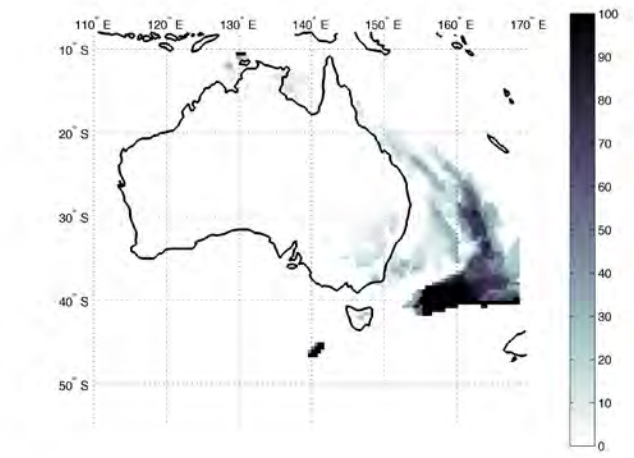
110° E
120° E
130° E
140° E
150° E
160° E
170° E
10° S
20° S
30° S
40° S
50° S
100
90
80
70
60
50
40
30
20
10
0

(c)

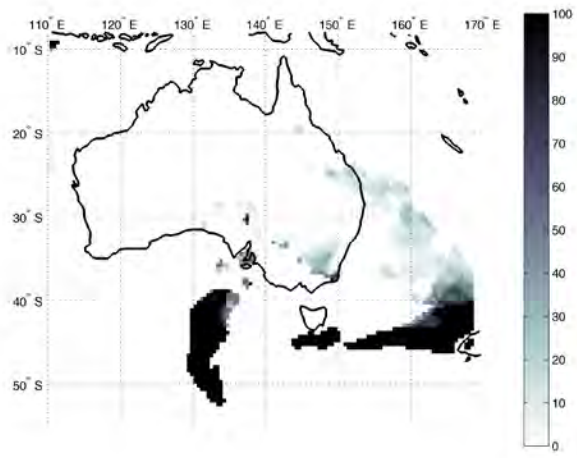
110° E
120° E
130° E
140° E
150° E
160° E
170° E
10° S
20° S
30° S
40° S
50° S
100
90
80
70
60
50
40
30
20
10
0

(d)

Fig. 6

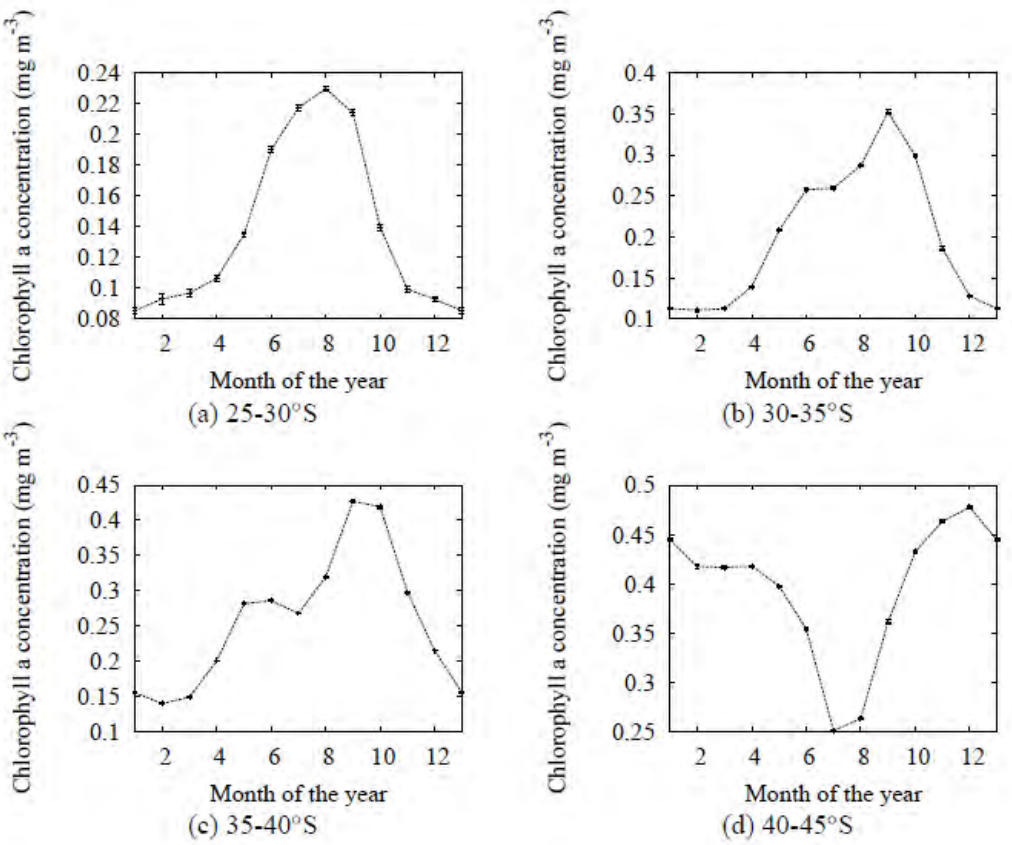
Chlorophyll a concentration (mg m-3)
Month of the year
(a) 25-30°S
(b) 30-35°S
(c) 35-40°S
(d) 40-45°S

Fig. 7

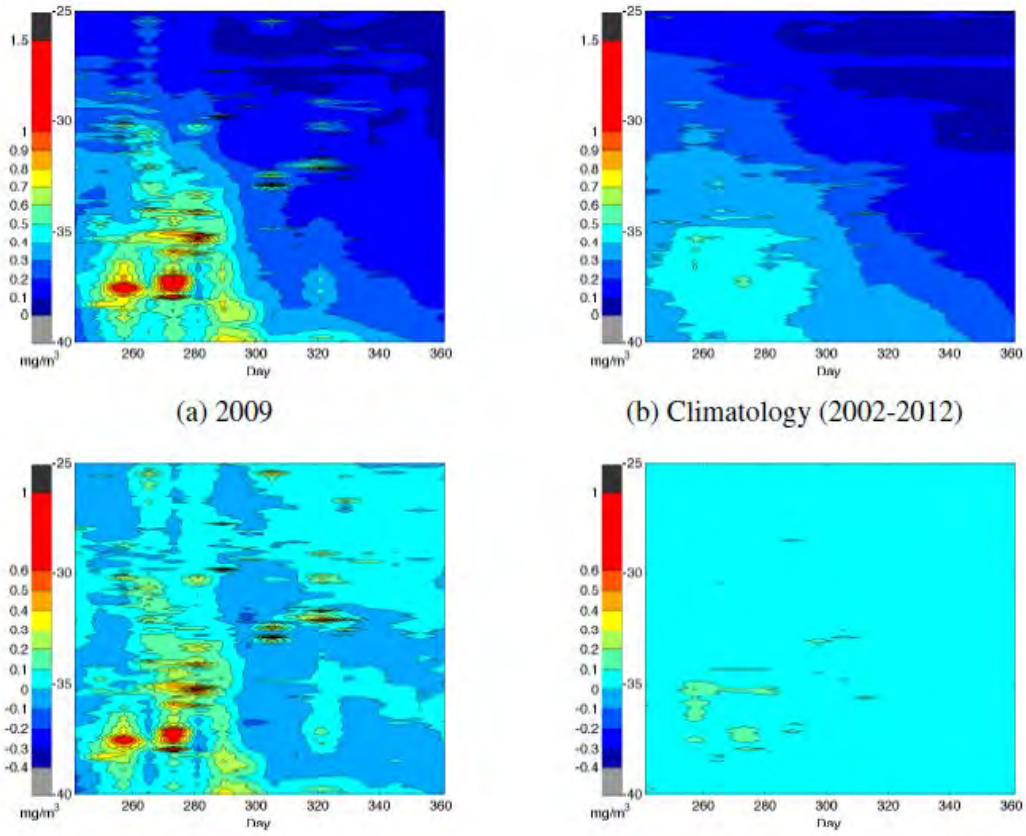
(a) 2009
(b) Climatology (2002-2012)
(c) The 2009 anomalies
(d) Standard error in climatology
mg/m3
Day

Fig. 8

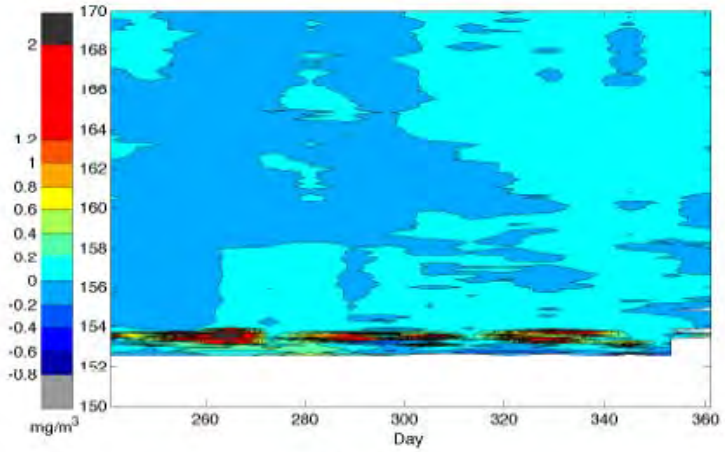

(a) 25-30°S

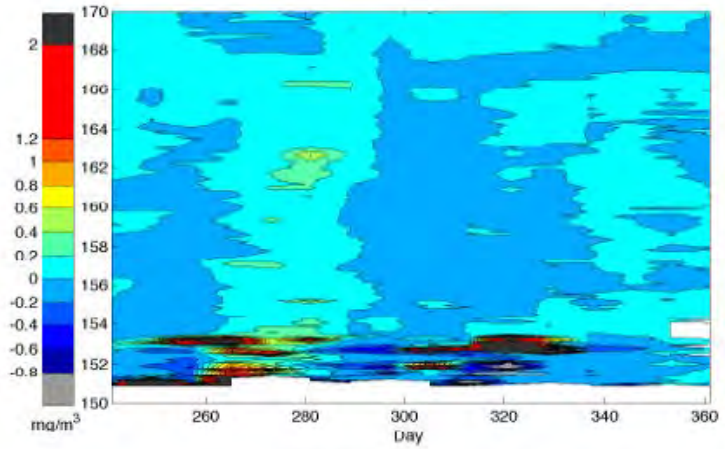

(b) 30-35°S

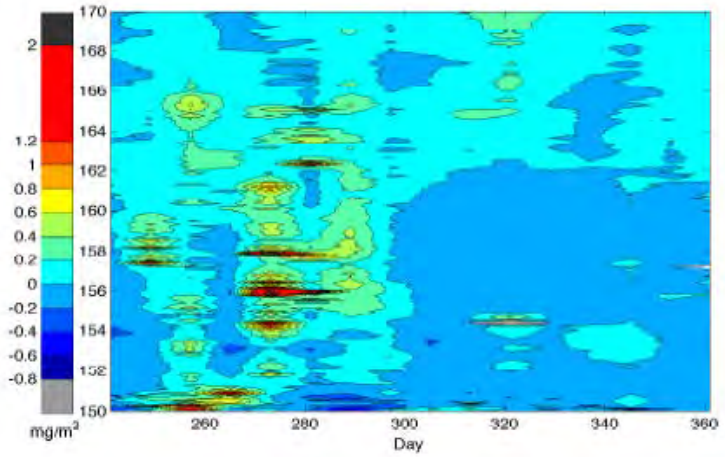

(c) 35-40°S

Fig. 9

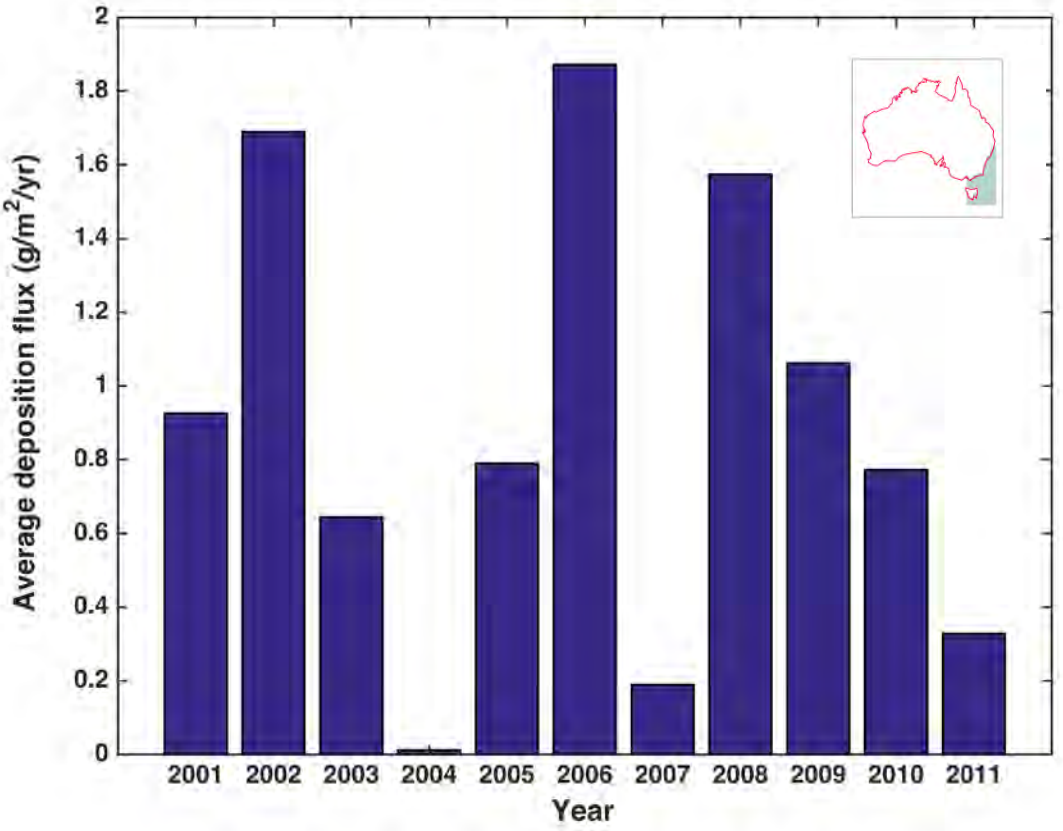
Average deposition flux (g/m^2/yr)
2
1.8
1.6
1.4
1.2
1
0.8
0.6
0.4
0.2
0
2001
2002
2003
2004
2005
2006
2007
2008
2009
2010
2011
Year

Fig. 10

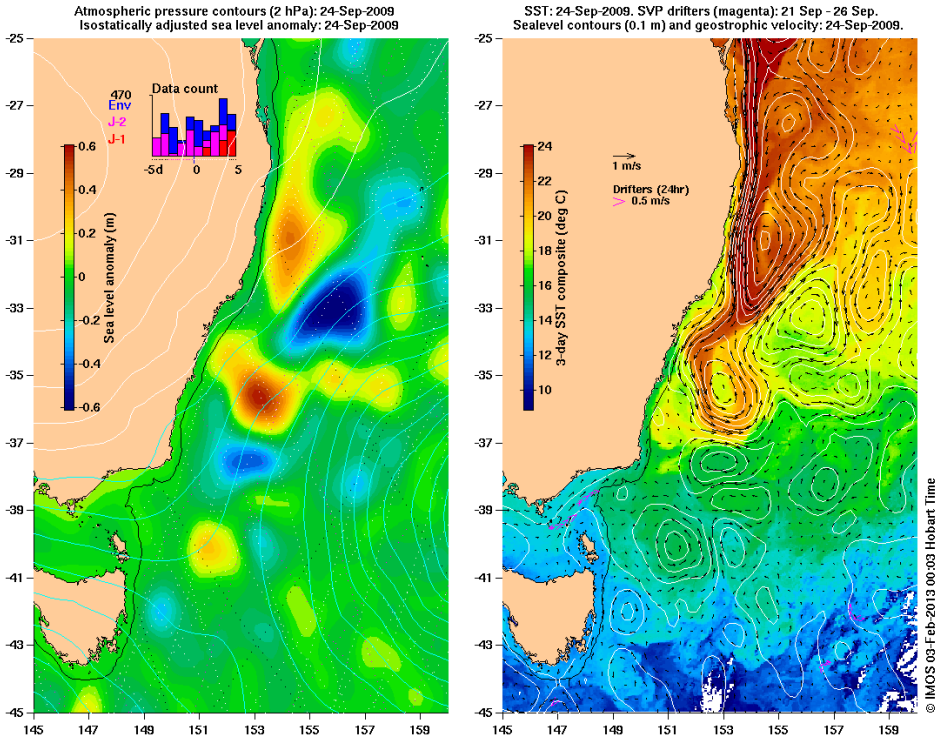
Atmospheric pressure contours (2 hPa): 24-Sep-2009
Isostatically adjusted sea level anomaly: 24-Sep-2009
470
Env
J-2
J-1
Data count
-5d
0
5
Sea level anomaly (m)
0.6
0.4
0.2
0
-0.2
-0.4
-0.6
SST: 24-Sep-2009. SVP drifters (magenta): 21 Sep - 26 Sep.
Sealevel contours (0.1 m) and geostrophic velocity: 24-Sep-2009.
1 m/s
Drifters (24hr)
> 0.5 m/s
3-day SST composite (deg C)
24
22
20
18
16
14
12
10
-25
-27
-29
-31
-33
-35
-37
-39
-41
-43
-45
145
147
149
151
153
155
157
159
© IMOS 03-Feb-2013 00:03 Hobart Time

Fig. 11

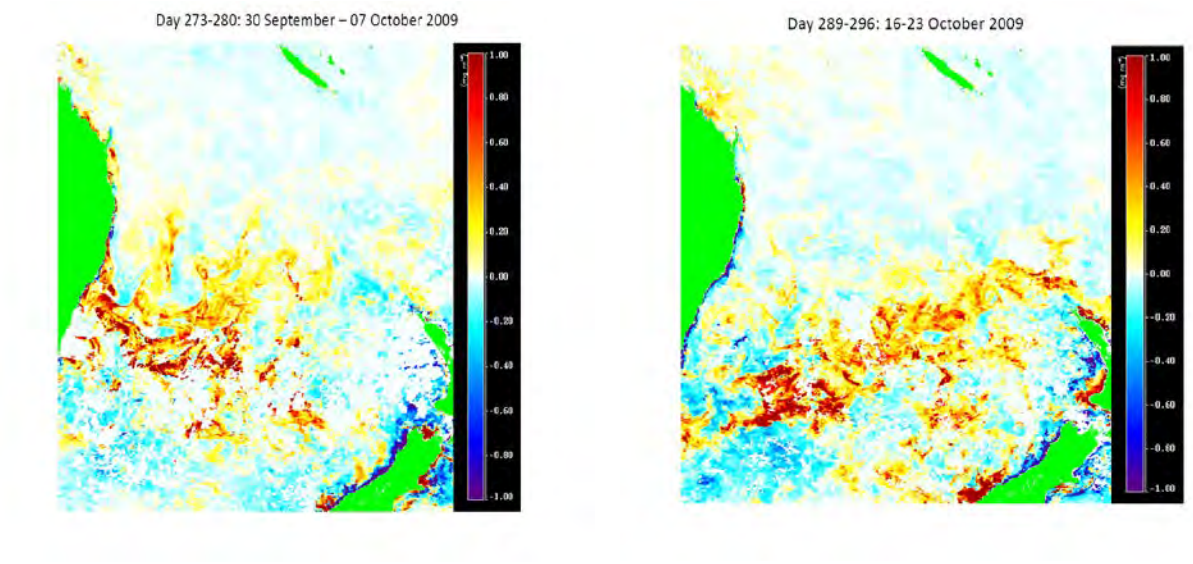
Day 273-280: 30 September – 07 October 2009
Day 289-296: 16-23 October 2009

(a) (b)

Fig. 12